ISSN: 0123-3033 – ISSN-e: 2027-8284
INGENIERIA Y COMPETITIVIDAD
REVISTA CIENTÍFICA Y TECNOLÓGICA
Vol. 23 No. 2-2021 - DOI: 10.25100/iyc.23i2.11262

MATERIALS ENGINEERING

Finite Element Analysis of Constrained Groove Pressing on Strain Behavior of Armco Iron Sheets

INGENIERÍA DE MATERIALES

Análisis por Elementos Finitos del Proceso de Presión Calibrada Restringida en la Deformación de Láminas de Hierro Armco

Oscar Fabián Higuera-Cobos[1§], Alejandro Mendoza-Cuesta[1], Yarib Suárez-Granados[1], Luis Carlos Flórez-García[2], Carlos Mauricio Moreno-Téllez[3]

[1]Universidad del Atlántico, Facultad de Ingeniería, Programa de Ingeniería Mecánica, Grupo de Investigación CONFORMAT, Barranquilla, Colombia

[2]Universidad Tecnológica de Pereira, Facultad de Ingeniería Mecánica, Grupo de Investigación CONFORMAT, Pereira, Colombia

[3]Universidad Pedagógica y Tecnológica de Colombia, Facultad de Ingeniería, Escuela de Ingeniería Metalúrgica, Grupo de Integridad y Evaluación de Materiales, Tunja, Colombia

[§]*oscarhiguera@mail.uniatlantico.edu.co, alejandromendoza@mail.uniatlantico.edu.co, ysuarezg@mail.uniatlantico.edu.co, louis@utp.edu.co, carlos.moreno@uptc.edu.co*

Recibido: 1 de febrero de 2021 – **Aceptado**: 27 de abril de 2021

Abstract

A comprehensive analysis of the elasto-plastic behavior of ARMCO iron sheets undergoing severe plastic deformation (SPD) by constrained groove pressing (CGP) was carried out via the finite element method (FEM). Parameters such as die geometry and coefficient of friction were considered to study its effects on the elasto-plastic response of the material. For this ANSYS workbench was used for FEM simulations. The results showed that the parameters studied influence in different ways not only the strain achieved but also the strain distribution through the sheet.

Keywords: *ARMCO iron, Constrained groove pressing, Effective strain, Finite element method.*

Resumen

Se llevó a cabo un análisis exhaustivo del comportamiento elastoplástico de láminas de hierro ARMCO sometidas a deformación plástica severa (SPD) mediante la técnica de presión calibrada restringida (CGP) por medio del método de elementos finitos (FEM). Se consideraron parámetros como la geometría de la matriz y el coeficiente de fricción para estudiar sus efectos en la respuesta elasto-plástica del material. Para ello se utilizó ANSYS workbench para las

Como citar:
Higuera-Cobos OF, Mendoza-Cuesta A, Suárez-Granados Y, Flórez-García C, Moreno-Tellez CM. Análisis por Elementos Finitos del Proceso de Presión Calibrada Restringida en la Deformación de Láminas de Hierro Armco. INGENIERÍA Y COMPETITIVIDAD. 2021;23(2):e21611262. https://doi.org/10.25100/iyc.v23i2.11262.

simulaciones por elementos finitos. Los resultados mostraron que los parámetros estudiados influyen de forma diferente no sólo en la deformación alcanzada sino también en la distribución de la deformación a través de la lámina.

Palabras clave: *Deformación efectiva, Hierro ARMCO, Método de elementos finitos, Presión calibrada restringida.*

1. Introduction

Bulk materials with ultrafine grain (UFG) sizes (a mean grain size between 100 nm and 1 μm) processed by severe plastic deformation (SPD) have attracted great interest from researchers in materials science. The lack of undesirable defects such as micro-porosities and their ability to be manufacture on a large scale grant them great potential for future industrial applications. In addition, UFG materials exhibit superior mechanical properties such as high strength, high toughness, good corrosion resistance, and superplasticity at high strain rates and low temperatures [(1-3)].

Over the years, several SPD techniques have been developed, of which equal channel angular pressing (ECAP) and high pressure torsion (HPT) are the most widely used [(4)]. There are other techniques for sheet metal processing such as accumulative roll-bonding (ARB), repetitive corrugating and straightening (RCS) and constrained groove pressing (CGP), where CGP stands out for its simplicity and practicality. CGP was developed by Shin et al. [(5)], who, in 2002, studied the microstructural behavior of pure aluminum, obtaining improvements on mechanical properties comparable to those obtained with other techniques under similar accumulated strains. Other researchers have studied the application of this technique on the microstructural and mechanical behavior of different materials such as low carbon steels, aluminum, and aluminum alloys, copper and copper alloys, magnesium alloys, nickel and titanium [(6)].

Figure 1 shows a schematic illustration of the CGP process. First, a sheet specimen is placed between a set of asymmetrically grooved dies, with a 45° groove angle (θ) and equally sized groove width and height (t) (Figure 1c). Pressing the dies against the sample results in pure shear deformation in the inclined region with an effective strain value of 0.58 (Figure 1d), this represents the first CGP cycle. For the second cycle, the sample is pressed against a set of flat dies, causing reverse shear deformation in the region previously deformed, which increases the effective strain up to 1.16 (Figure 1e). For the third cycle, the sample is rotated 180° around an axis perpendicular to the plane of the sample (Figure 1f).

The same procedure for the first and second cycle is repeated, which results in a homogeneous effective strain of 1.16 throughout the sample. This is equivalent to four CGP cycles or one CGP pass. Eqs. 1 - 6 represent the mathematical procedure for determining the imposed effective strain in the inclined region of the sheet after the first cycle [(8,9)].

Engineering shear strain is defined as,

$$\gamma_{xy} = \frac{\Delta x}{t} = \tan\theta \quad (1)$$

Thereby, shear strain is given as,

$$\varepsilon_{xy} = \frac{\gamma_{xy}}{2} \quad (2)$$

Then, the Von Mises effective strain ε_{eff} is given by,

$$\varepsilon_{eff} = \sqrt{\frac{2}{9}\left[(\varepsilon_x - \varepsilon_y)^2 + (\varepsilon_y - \varepsilon_z)^2 + (\varepsilon_z - \varepsilon_x)^2\right] + \frac{4}{3}\left[\varepsilon_{xy}{}^2 + \varepsilon_{yz}{}^2 + \varepsilon_{zx}{}^2\right]} \quad (3)$$

Assuming the deformation as simple shear with no longitudinal and transverse expansion,

$$\varepsilon_x = \varepsilon_y = \varepsilon_z = \varepsilon_{yz} = \varepsilon_{zx} = 0 \quad (4)$$

$$\varepsilon_{eff} = \sqrt{\frac{4(\gamma_{xy}/2)^2}{3}} \quad (5)$$

$$\varepsilon_{eff} = \frac{\tan\theta}{\sqrt{3}} \quad (6)$$

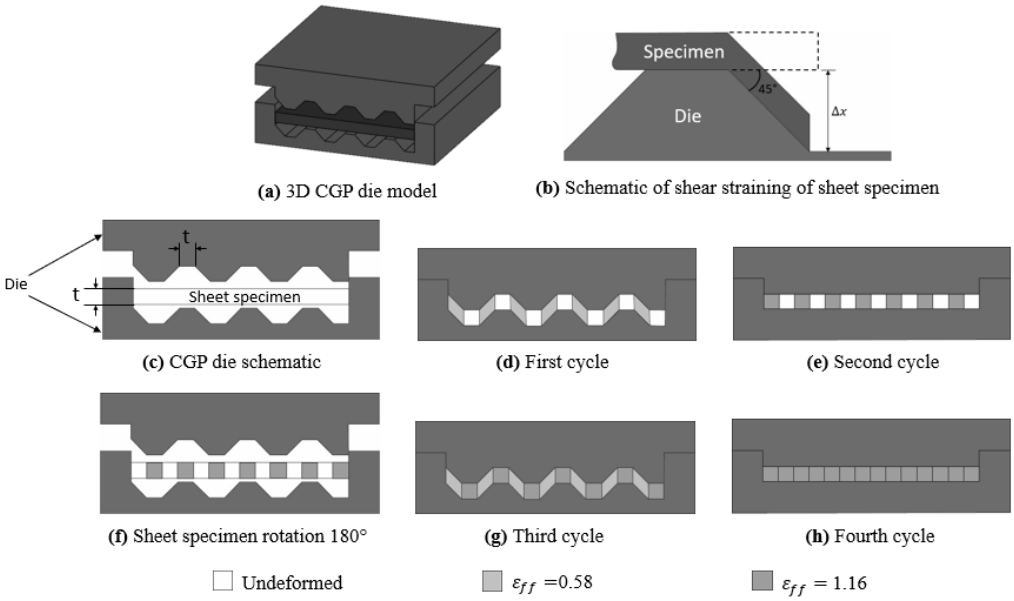

Figure 1. *Schematic illustration of CGP process* [6,7]

Research activities rely on two important components: theoretical and experimental. Computer simulations are a widely used tool by researchers in many fields of study to emulate physical experiments, which, when properly modeled, allow results to be obtained more quickly and in a cost-effective fashion with acceptable levels of accuracy comparable to those obtained experimentally. One of the most popular computer simulation methods is the finite element method (FEM).

Many authors have employed FEM in their studies to analyze in depth the behavior of materials processed by CGP. Focusing primarily on the effect of die geometry on material strain distribution, Yoon et al. [10] studied the strain variations along the longitudinal direction during the application of CGP in pure cooper, obtaining greater strain heterogeneity by increasing the number of cycles. Sajadi et al. [7] analyzed the effect of three CGP die designs on mechanical and microstructural behavior of pure aluminum; while Wang et al. [11] performed a similar study but analyzing in depth the influence of die geometry on the mechanical and microstructural behavior of pure Nickel. Besides, several studies on the effect of friction in CGP process have been conducted, like Wang et al. [12] who investigated the influence of lubrication on mechanical and microstructural behavior of pure aluminum.

FCC metals deform via slip and twinning, due to their lower stacking fault energy as compared to BCC crystals. This is the primary reason why severe plastic deformation of FCC metals has been widely investigated throughout literature. Pure Iron, in contrast, has a BCC crystal structure at room temperature. These materials do not possess slip systems with truly closed-packed planes whereby dislocation motion could take place through the crystal lattice, hence, plastic deformation is not the preferred method for the enhancement of their mechanical properties. The improvement of the mechanical properties of these materials through SPD techniques represents a challenge. Therefore, the optimization of the process is required. This work seeks to carry out a comprehensive analysis of two critical factors in the CGP process: friction conditions and die geometry.

2. Methodology

2.1. Finite element procedure

The commercial finite element code, Ansys/Static structural software was used to investigate the elasto-plastic response and the effects on the mechanical properties of ARMCO iron during the application of severe plastic deformation by CGP. A 2D plastic strain model was used to reduce computational time. Table 1 shows the geometrical variations used for the first CGP cycle simulations. These were used to study the strain behavior when groove width (t) and angle (θ) were varied. Besides, the response due to variations in the coefficient of friction (0, 0.15, and 0.3) for $\boldsymbol{D_3}$ model was studied.

Table 1. *Geometric variations*

		$\boldsymbol{\theta}$		
		30°	45°	60°
t [mm]	1		D_1	
	2	D_2	D_3	D_4
	3		D_5	

2.2. Material model

A 2 mm thickness ARMCO iron sheet was used (see Table 2). To reduce simulation time dies typically manufactured in D_2 steel were simulated as rigid bodies. In addition, an isotropic bilinear hardening model was used to model the plastic behavior of ARMCO iron with a tangent modulus of 446 MPa.

2.3. Meshing and contact conditions

An ARMCO iron sheet was meshed using a bilinear flat quadrilateral model with a nonlinear adaptive region, to model the large deformation that takes place in the process. Contact conditions were set as frictional except for the case with a coefficient of friction equal to zero, where the contact was modeled as frictionless.

Table 2. *Properties of Armco iron*

Properties	Value
Density at 20°C	7.86 Kg/dm^3
Modulus of elasticity	207 GPa
Poisson's ratio	0.3
Compressibility Module	172.5 GPa
Shear Module	79.6 GPa
Yield point	186 MPa

3. Results and discussion

3.1. Groove angle variation

Figure 2 shows the effective strain for groove angle variations. Significant changes in the strain behavior for the inclined region of the sheet were observed at different groove angles.

$\boldsymbol{D_2}$ model exhibited a higher strain concentration in the center of the inclined region, with a maximum strain value of approximately 0.33, which gradually decreases until a value of 0.14 in the upper and lower ends of the sheet. $\boldsymbol{D_4}$ model exhibited greater strain uniformity along the inclined region than $\boldsymbol{D_2}$ model, with a maximum value of approximately 0.82, but this time farther from the center and located closer to the interface (junction between flat and inclined regions), decreasing to a value of 0.63 in areas much closer to the interface. $\boldsymbol{D_3}$ model presented a similar behavior to $\boldsymbol{D_4}$ model, i.e., greater strain uniformity with respect to $\boldsymbol{D_2}$ model.

Rezaei et al. [13] reported a similar behavior in their study on groove pressing applied to pure aluminum in which groove angle variations between 40 to 50° showed an increase in effective strain with increasing groove angle. Strain distribution simulation for the 50° groove angle

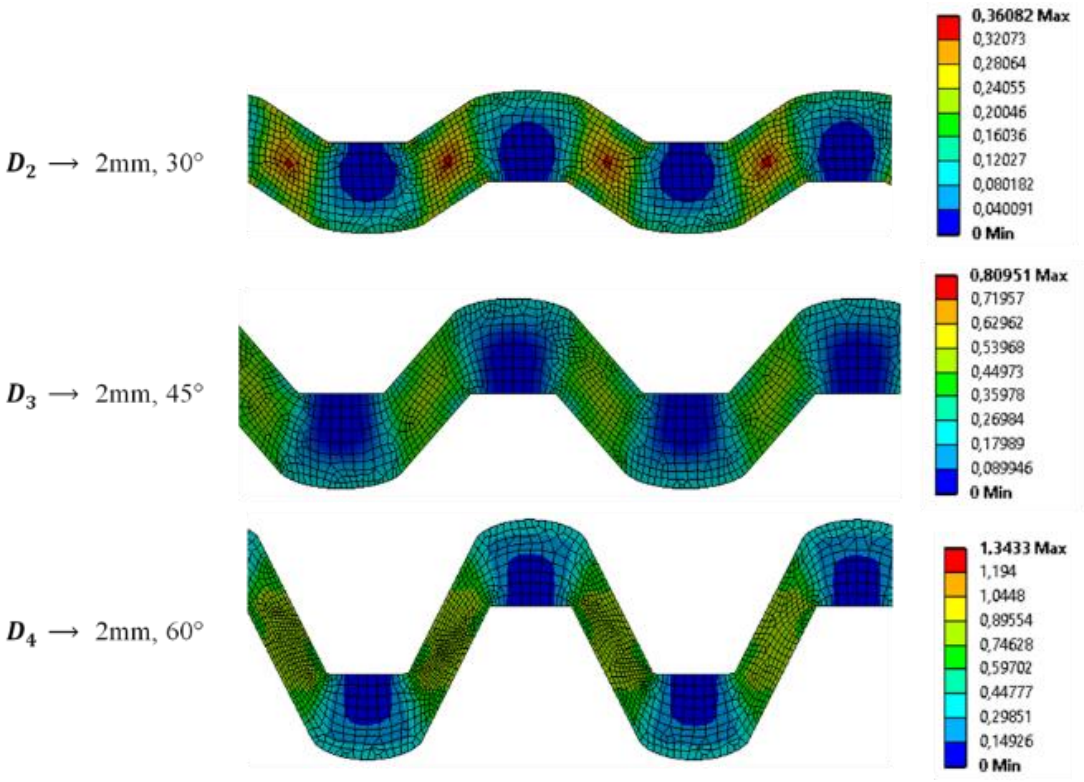

Figure 2. *Effective strain simulation for groove angle variations*

presented less uniformity than that obtained by the 40° groove angle. They attributed this behavior to the fact that an increase in groove angle causes the inclined region to be subjected not only to shear stress but tensile stress too. Sajadi et al. [(7)] also reported the same behavior in their study on the effects of CGP on pure aluminum. After the first flattening (Figure 1e), they observed higher strain levels when varying groove angle from 45 to 53°, being the 45° die the one with the highest strain uniformity between both. Borhani and Djavanroodi [(14)] found the same behavior for pure aluminum subjected to rubber pad–constrained groove pressing, in which a less uniform strain distribution was found for a 50° groove angle die compared to a 45° one.

The studies mentioned above only took into account groove angles greater than 40°, on the other hand, Wang et al. [(11)] studied the strain behavior of pure nickel sheets subjected to CGP with groove angle variations from 30 to 60°; it was found that sheets deformed with a 60° groove angle exhibited a less uniform strain behavior to the others. This is because at 60° the deformation process behaves like that of forging, and bending deformation starts to occur, achieving higher strain values and possible damage to the sheet. This behavioral change in deformation mode occurs at groove angle values close to 50.8° as reported in [(11)]. Figure 3 shows the groove angle influence on strain behavior. Indeed, the mean effective strain value increase with every groove angle increase. However, unusual behavior was observed for the standard deviation (SD) of effective strain. This represents the strain uniformity in the inclined region of the sheet. D_3 and D_2 model presented the highest and lowest strain uniformity, respectively; similar results were obtained by Wang et al. [(11)] for a 45° groove angle die.

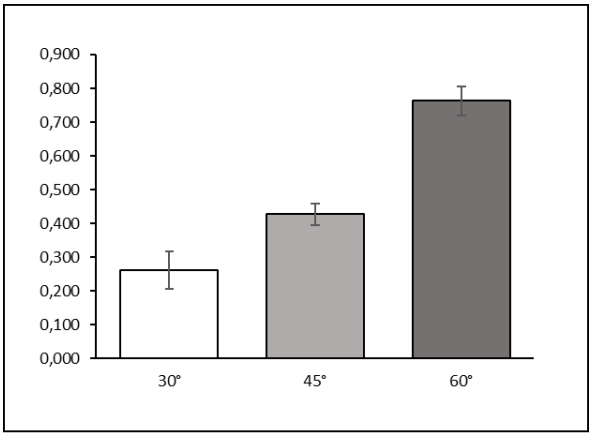

Figure 3. *Effective strain means and standard deviation for groove angle variations*

3.2. Groove width variation

Figure 4 shows the effective strain simulation for groove width variations. In general terms, $\boldsymbol{D_1}$, $\boldsymbol{D_3}$ and $\boldsymbol{D_5}$ models presented similar maximum strain values; with maximum strain values of approximately 0.49, 0.47, and 0.45, respectively. When groove width increases, fewer strain levels are obtained. Figure 5 shows the effective strain mean and standard deviation for groove width variations. The mean effective strain values obtained showed an inverse relation between groove width and effective strain. Wang et al. [(11)] found a similar relation for different groove widths from 1 to 4 mm. However, their effective strain results varied substantially from one another, from 0.815 to 0.64. This differs from what was found in this work, in which little variation occurred. Eq. 6 may provide an explanation. In it, effective strain is modeled as a function of groove angle and it does not take into account the effect of groove width variations.

The standard deviation of effective strain in the inclined region of the sheet showed in Figure 5 shows that D_3 model exhibits greater strain uniformity than the other two (as seen by the decrease in SD). Although the effective strain becomes more uniform from D_1 to D_3 model, which corresponds to an increase from 1 to 2 mm groove width, the opposite is true from D_3 to D_5 model that is from 2 to 3 mm groove width (as seen by the increase in SD). Wang et al. [(11)] showed that if the ratio of groove width to sample thickness is less than 1.25, then a stable shear strain throughout the sheet can be ensured; thus, for a 3 mm groove width and a sample thickness of 2 mm, a ratio of 1.5 is involved, which is greater than the limit of 1.25. This explains the decrease in strain uniformity found for D_5 model.

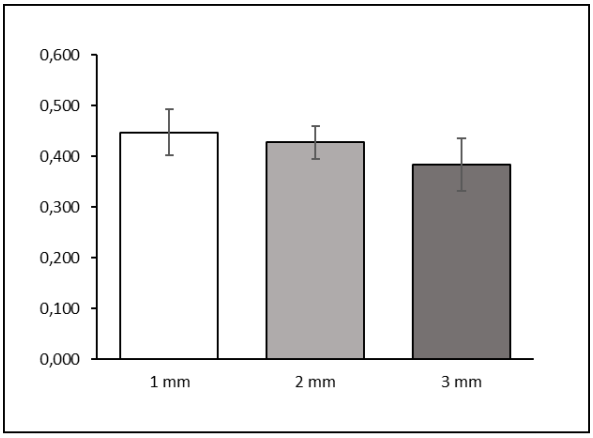

Figure 4. *Effective strain means and standard deviation for groove width variations*

It should note that the maximum strain values reported in Figures 2 and 4 far exceed the maximum values found for the inclined region of the sheet. These peak strains located along the regions near the edges of the sheet were dismissed from analysis as outliers.

3.3. Variation in the coefficient of friction

The values used for the coefficient of friction (0, 0.15, and 0.3) chosen to emulate the conditions of non-friction, MoS_2 lubrication, and metal-metal contact, respectively. Figure 6 shows the selected area of the sample under analysis, which dismisses the unwanted effects of boundary conditions and focuses only on the central sheet region. The strain distribution for the surface and central node paths were obtained.

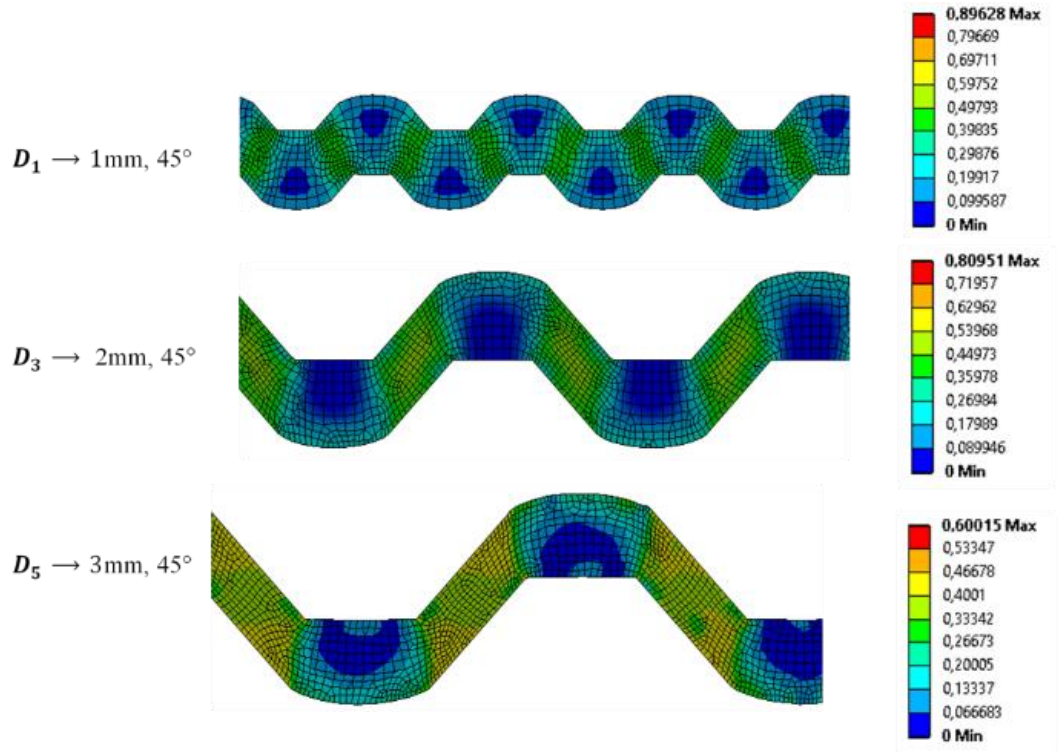

Figure 5. *Effective strain simulation for groove width variation*

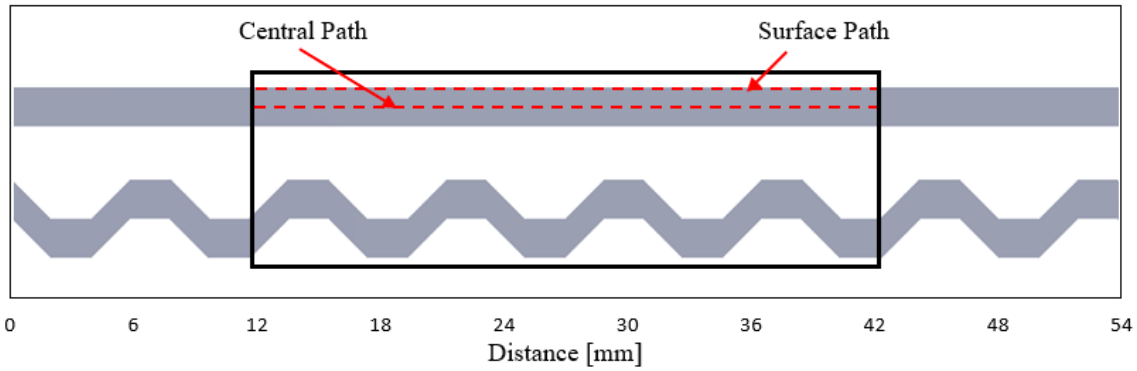

Figure 6. *Selected area for analysis*

Figure 7 shows the strain distribution for the central node path. The curve takes the form of a sinusoid wave, with a wavelength of twice the sample thickness.

This behavior is because, at inclined regions, the effective strain is maximum, reaching values of around 0.5, while at flat regions it drops near to zero. It can be seen that at higher coefficient of friction, higher strain values are obtained, showing a slight but noticeable effect, as Wang et al. [(12)] also reported in a similar study. As expressed before, the effective strain does not drop completely to zero in flat regions. However, theoretically, the induced strain at inclined regions does not affect their flat counterparts. This idealized behavior does not occur, and a certain amount of strain induced, which can be seen as the small value presented in Figure 8. Yoon et al. [(10)] and Peng et al. [(15)] also found that the interface between flat and inclined region plays an important role on strain distribution.

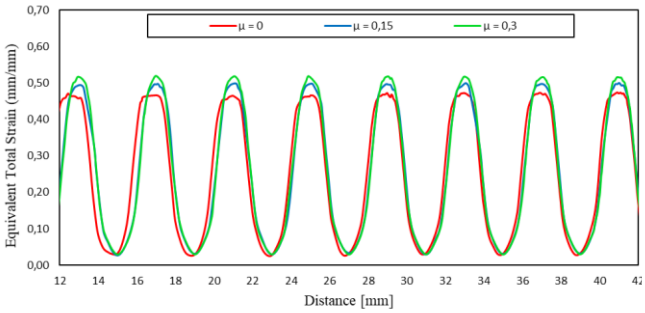

Figure 7. *Strain distribution for Central Path*

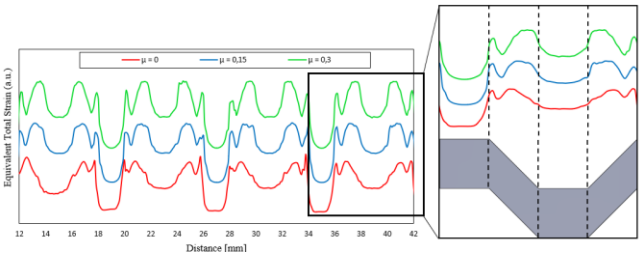

Figure 8. *Strain distribution for Surface Path*

Figure 8 shows the strain distribution for surface node path, this path experiences a more complicated strain distribution curve compared to the central path, although it still preserves its periodical nature, this time repeating itself along the sheet every 8 mm. The zoom in section in Figure 8 shows how the strain distribution curve changes along the different regions of the sheet. The upper flat region does not present much strain since it is not meant to be deformed at all, however, the same cannot be said for its lower flat counterpart. Even though theoretically this region should not experience any deformation either; simulation results show a near constant non-zero value at its surface because of die groove being pressed on it. The inclined regions present a mirror pattern of each other due to their symmetry. The curves present two distinctive crests, a little one at the interface between flat and inclined region, and a more pronounced one at the center of the inclined region.

As well as with the central path, the surface path strain values increase when increasing the coefficient of friction alongside with an increase in strain uniformity. However, this increase in strain uniformity is relative as there is a marked difference between the surface and central path strain behavior, which was also reported by Kumar et al. [16] who found different strain patterns not only between the surface and central path but also between the top and bottom surfaces themselves, also compromising the grain refinement homogeneity.

4. Conclusions

The influence of die geometry and friction on the elasto-plastic response of ARMCO iron sheets deformed via CGP was investigated through finite element method. It was found that groove width and angle variations have a considerable impact on the strain distribution of the material.

As groove angle increases, a higher effective strain is found and the deformation behavior of the material gains uniformity from 30 to 45° (D_2 to D_3 model) but becomes less uniform at 60° (D_4 model) because a limiting angle of about 50.8° is surpassed and pure shear strain is no longer the only mode of deformation present in the sample as bending deformation starts to play a role. Besides, as groove width increases, a lower effective strain is found and the deformation behavior of the material gains uniformity from 1 to 2 mm (D_1 to D_3 model) but becomes less uniform at 3 mm (D_5 model) as the groove width to sample thickness ratio limit of 1.25 is exceeded and thereafter a stable shear strain cannot be attained throughout the sheet.

The strain distribution curves for different friction conditions for the central region and upper surface of the sheet showed that when increasing the coefficient of friction, the deformation throughout the sheet increased by a small amount and its strain uniformity decreases.

5. Acknowledgement and/or Funding Statement

The authors thank the Universidad del Atlántico for funding ING16-TGI2018 project. The authors also thank the support of CNCA-SENA during implementation of the severe plastic deformation by CGP, especially Eng. Hugo González.

6. References

(1) Valiev RZ, Alexandrov IV, Zhu YT, Lowe TC. Paradox on of strength and ductility in metals processed by SPD. J. Mater. Res. 2002;17 :5–8. https://doi.org/10.1557/JMR.2002.0002

(2) Zhu YT, Langdon TG. The fundamentals of nanostructured materials processed by severe plastic deformation. JOM. 2004; 56(10): 58–63. https://doi.org/10.1007/s11837-004-0294-0

(3) Sabirov I, Murashkin MY, Valiev RZ. Nanostructured aluminium alloys produced by severe plastic deformation: New horizons in development. Mater. Sci. Eng. A. 2013; 560:1–24. https://doi.org/10.1016/j.msea.2012.09.020

(4) Figueiredo RB, Langdon TG. Fabricating ultrafine-grained materials through the application of severe plastic deformation: A review of developments in Brazil. J. Mater. Res. Technol. 2012; 1(1):55–62. https://doi.org/10.1016/S2238-7854(12)70010-8

(5) Shin DH, Park JJ, Kim YS, Park KT. Constrained groove pressing and its application to grain refinement of aluminum. Mater. Sci. Eng. A. 2002; 328(1-2):98–103. https://doi.org/10.1016/S0921-5093(01)01665-3

(6) Gupta AK, Maddukuri TS, Singh SK. Constrained groove pressing for sheet metal processing. Prog. Mater. Sci. 2016; 84:403–462.https://doi.org/10.1016/j.pmatsci.2016.09.008

(7) Sajadi A, Ebrahimi M, Djavanroodi F. Experimental and numerical investigation of Al properties fabricated by CGP process. Mater. Sci. Eng. A. 2012; 552:97–103. https://doi.org/10.1016/j.msea.2012.04.121

(8) Niranjan GG, Chakkingal U. Deep drawability of commercial purity aluminum sheets processed by groove pressing. J. Mater. Process. Technol. 2010; 210(11):1511–1516. https://doi.org/10.1016/j.jmatprotec.2010.04.009

(9) Shirdel A, Khajeh A, Moshksar MM. Experimental and finite element investigation of semi-constrained groove pressing process. Mater. Des. 2010; 31(2):946–950. https://doi.org/10.1016/j.matdes.2009.07.035

(10) Yoon SC, Krishnaiah A, Chakkingal U, Kim HS. Severe plastic deformation and strain localization in groove pressing. Comput. Mater. Sci. 2008; 43(4):641–645. https://doi.org/10.1016/j.commatsci.2008.01.007

(11) Wang ZS, Guan YJ, Wang GC, Zhong CK. Influences of die structure on constrained groove pressing of commercially pure Ni sheets. J. Mater. Process. Technol. 2015; 215(1): 205–218. https://doi.org/10.1016/j.jmatprotec.2014.08.018

(12) Wang ZS, Guan YJ, Zhong CK. Effects of Friction on Constrained Groove Pressing of Pure Al Sheets. Adv. Mater. Res. 2014; 926-

930 :81-84. https://doi.org/10.4028/www.scientific.net/AMR.926-930.81.

(13) Rezaei-Ashtiani HR, Aradpur S, Rafiei M. The Effect of Groove Angles on Groove Pressing Process. In: International Conference on Mechanical Engineering and Advanced Technology. 2012; October 10-12; Isfahan, Iran.

(14) Borhani M, Djavanroodi F. Rubber pad-constrained groove pressing process: Experimental and finite element investigation. Mater. Sci. Eng. A. 2012; 546:1-7. https://doi.org/10.1016/j.msea.2012.02.089

(15) Peng K, Mou X, Zeng J, Shaw LL, Qian KW. Equivalent strain, microstructure and hardness of H62 brass deformed by constrained groove pressing. Comput. Mater. Sci. 2011; 50(4):1526-1532. https://doi.org/10.1016/j.commatsci.2010.12.010

(16) Kumar S, Hariharan K, Digavalli RK, Paul SK. Accounting Bauschinger effect in the numerical simulation of constrained groove pressing process. J. Manuf. Process. 2019; 38:49–62. https://doi.org/10.1016/j.jmapro.2018.12.013.